Review of Scientific Instruments

Determining local modulus and strength of heterogeneous films by force–deflection mapping of microcantilevers

Cite as: Rev. Sci. Instrum. **94**, 033904 (2023); https://doi.org/10.1063/5.0092934
Submitted: 24 March 2022 • Accepted: 19 February 2023 • Published Online: 10 March 2023

Kyle Larsen, Stefan Lehnardt, Bryce Anderson, et al.

AIP Publishing

Review of Scientific Instruments ARTICLE scitation.org/journal/rsi

Determining local modulus and strength of heterogeneous films by force–deflection mapping of microcantilevers

Cite as: Rev. Sci. Instrum. 94, 033904 (2023); doi: 10.1063/5.0092934
Submitted: 24 March 2022 • Accepted: 19 February 2023 •
Published Online: 10 March 2023

Kyle Larsen, Stefan Lehnardt, Bryce Anderson, Joseph Rowley, Richard Vanfleet, and Robert Davis[a]

AFFILIATIONS

Department of Physics and Astronomy, Brigham Young University, Provo, Utah 84604, USA

[a]Author to whom correspondence may be addressed: davis@byu.edu

ABSTRACT

Estimating the elastic modulus and strength of heterogeneous films requires local measurement techniques. For local mechanical film testing, microcantilevers were cut into suspended many-layer graphene using a focused ion beam. An optical transmittance technique was used to map thickness near the cantilevers, and multipoint force–deflection mapping with an atomic force microscope was used to record the compliance of the cantilevers. These data were used to estimate the elastic modulus of the film by fitting the compliance at multiple locations along the cantilever to a fixed-free Euler–Bernoulli beam model. This method resulted in a lower uncertainty than is possible from analyzing only a single force–deflection. The breaking strength of the film was also found by deflecting cantilevers until fracture. The average modulus and strength of the many-layer graphene films are 300 and 12 GPa, respectively. The multipoint force–deflection method is well suited to analyze films that are heterogeneous in thickness or wrinkled.

I. INTRODUCTION

Here we will describe a method for characterizing the local mechanical properties of heterogeneous thin films, which we call multipoint force–deflection (MFD). We will analyze the applicability of this method to characterizing many-layer graphene (MLG) films that are heterogeneous in thickness and contain wrinkles. Bulge testing is a common method for measuring the tensile strength and elastic modulus of suspended thin films.[1] With wrinkled or non-uniform films, the bulge test method can be used to determine deflection and burst pressure; however, it cannot quantitatively determine modulus or strength. The force–deflection or beam bending method is another established technique for determining material properties by applying a force to a microcantilever and measuring its deflection,[2] which can be done using an atomic force microscope (AFM).[3,4] These small cantilevers make it possible to target specific locations on a film, thereby enabling measurements on local regions. For example, it is possible to measure over a range of thicknesses or to target areas devoid of wrinkles. Traditionally, the force–deflection method involves measuring the deflection from a known force at a single point along the cantilever. The Euler–Bernoulli beam theory is then used to extract Young's modulus. A limitation of this technique is that an independent measurement of the distance from the applied force to the cantilever's fixed end is required. Both the location of the applied force and the type of boundary condition at the cantilever's fixed end can be difficult to determine. Here, we introduce a modification to this technique that does not require an independent measurement of the distance from the applied force to the cantilever's fixed end. This modification involves sequentially deflecting the cantilever at multiple locations along its length (see Fig. 1) and fitting both Young's modulus and the distance from the cantilever's fixed end. Similar works for determining Young's modulus using AFM force–deflection mapping have been reported previously for films suspended over circular holes[5–8] and for fibers, modeled as doubly clamped beams.[9,10] The singly clamped cantilever beam has the advantage that only one fixed edge is required, increasing the utility of the method by possibly simplifying the fabrication process. All of these techniques require knowing the thickness of the film, which is of critical importance in determining Young's modulus with cantilever bending because the modulus depends on the value of thickness to the third power. Various methods exist for measuring

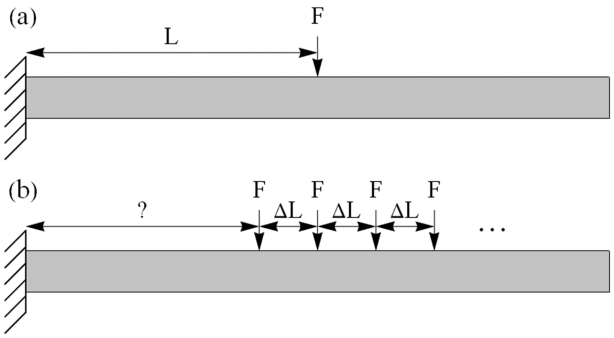

FIG. 1. Side-view schematic of cantilevers showing different force–deflection methods. (a) With single-point force–deflection, the location of the applied force relative to the fixed end must be known. (b) With multipoint force–deflection, the location of the applied forces to the fixed end is estimated through fitting.

the thickness of thin films, including ellipsometry, cross-sectional electron microscopy, and AFM step height measurement; however, these methods are all incompatible with the high-resolution thickness mapping necessary for local force–deflection measurements. We use an optical transmittance mapping technique for determining MLG film thickness. We use finite element modeling to confirm the applicability of the analytical Euler–Bernoulli beam theory to analyzing the MFD data. This work reports for the first time how AFM force–deflection mapping of microcantilevers can be used in combination with optical thickness mapping to estimate local Young's modulus of heterogeneous films.

Many-layer graphene is a thin film with tens to hundreds of graphitic layers. Graphitic carbon of this thickness is often called ultrathin graphite; however, we have chosen to use the term many-layer graphene because the films are grown using the same chemical vapor deposition (CVD) methods that produce monolayer, few-layer, or multilayer (up to ten layers) graphene. Graphene has a reported Young's modulus of 1 TPa[6,11,12] and an ultimate tensile strength of up to 130 GPa.[6] Despite this high strength, monolayer to multilayer graphene films are too thin to be directly suitable for many microelectromechanical systems (MEMS) and larger-scale mechanical applications. MLG is an attractive mechanical material that has been used to demonstrate loudspeakers[13] and x-ray detector windows.[14–17] However, the characterization of the mechanical properties of MLG films has been limited. The characterization of MLG films can be complicated by large wrinkles and significant thickness heterogeneity. Both of these problems can be minimized with a local characterization method, such as MFD, and with a local thickness measurement. In the case of MLG, the thickness can be determined locally with optical transmittance.[18,19]

In this work, we show the applicability of the MFD method to analyzing wrinkled MLG films with thickness non-uniformity. Young's modulus was estimated from AFM force–volume mapping on ion-cut MLG microcantilevers. While ion-cutting had the advantage of allowing us to characterize films that were already suspended over large apertures, it also appeared to cause damage in the surrounding films. Although only discussed here briefly, other microfabrication techniques can be used to create the cantilevers without this limitation. Additionally, several cantilevers were loaded until fracture to determine their breaking strength. The thickness was measured using optical transmittance and AFM step height measurements. Our use of multipoint force–deflection shows improvements over single-point force–deflection and bulge testing by eliminating the need for an independent measurement of the fixed end location, by giving insight into the validity of the model and boundary condition assumptions, and by enabling the measurement of local film properties. Additionally, this technique is valuable for the analysis of other suspended thin films, especially heterogeneous films that are traditionally difficult to characterize by bulge testing.

II. MATERIALS AND METHODS

A. Finite element modeling of cantilever beams

The multipoint force–deflection method was explored with finite element modeling (FEM) using COMSOL Multiphysics. Three simple models were developed to test slightly different boundary conditions (see Fig. 2) and to determine whether the one-dimensional Euler–Bernoulli model is applicable along the midline to cantilevers with our dimensions. In the first model, the end was fixed as is typical for a fixed-free cantilever beam. In the second model, the end was extended over a fixed surface to represent well-adhered MLG over silicon. The third model, representing poorly adhered MLG over silicon, combined the fixed end of the first model and a simple support at the edge of the silicon. In the second and third models, the region extending over the silicon is half the total cantilever length L_0. The first two models were expected to give similar force–deflection results. In fact, the expectation was that the second model would be close enough to the first to justify using the simpler fixed-free analytical model to analyze the collected force–deflection data. The third model was developed to represent a poorly adhered cantilever, which is useful in showing how different the deflection results are when the fixed end boundary condition is not achieved. All three models used the same length $L_0 = 3\ \mu$m,

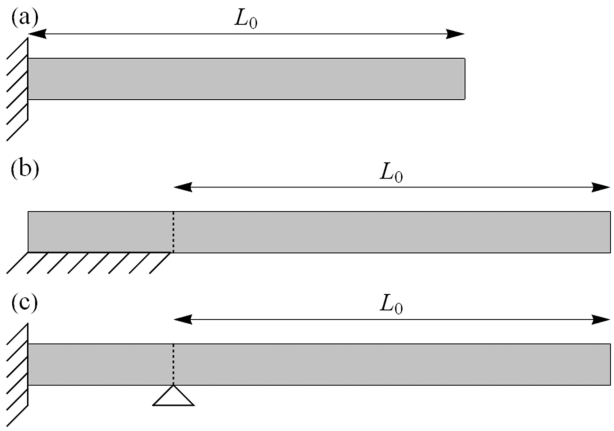

FIG. 2. Side-view schematic of three cantilever boundary conditions. (a) Cantilever with classically fixed end, referred to as BC 1. (b) Cantilever fixed to a silicon support, referred to as BC 2. (c) Similar to (b) but not well adhered to silicon, referred to as BC 3. The length L_0 is the same for all three cases.

width $w = 1\ \mu$m, thickness $t = 160$ nm, and material properties. The modulus was defined as $E_{FEM} = 1$ TPa. To test the MFD method, each of these models had a series of equally spaced point loads applied sequentially along the centerline of the cantilever, from the fixed end to the free end. The force–deflection results were then analyzed with the same technique that was used to analyze the AFM force–volume data. This technique is described later.

B. Sample preparation

The MLG films were formed using a low-pressure chemical vapor deposition (LPCVD) process on a nickel substrate.[13,17] Each film was then transferred to a silicon chip with an etched rectangular hole using a polymer assisted transfer process,[20] resulting in suspended MLG over the hole. The silicon support frame allows for the film to be suspended and for the cantilevers to be cut into the suspended film. The etched rectangular holes ranged in width from 100 to 500 μm, with the length being six times the width. For details on the growth and transfer process, see the supplementary material of this paper.

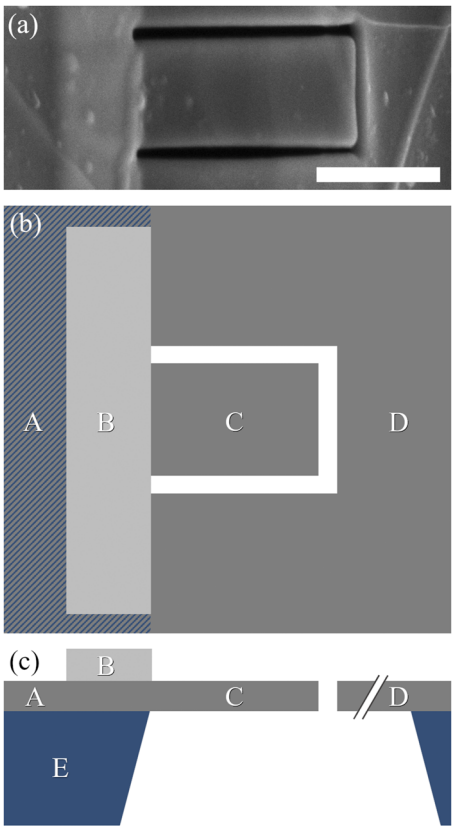

FIG. 3. Geometry of a many-layer graphene cantilever. (a) Scanning electron micrograph of a cantilever cut into suspended MLG, with the fixed end at the edge of the silicon support and stiffened by platinum. The scale bar is 1 μm long. (b) Top view schematic of a cantilever cut into suspended many-layer graphene. In region (A), the MLG is over the silicon support structure. Region (B) is the platinum bar that is e-beam deposited at the fixed end of the cantilever. The cantilever itself is region (C); it, along with region (D), is on the suspended MLG. (c) Side-view schematic of a cantilever cut into suspended MLG. The letters represent the same regions as in (b), with (E) indicating the silicon support frame. The opening in the silicon support frame is much larger than the length of the cantilever and hence the scale break mark near (D).

A series of MLG cantilevers was formed by cutting the suspended MLG film with a focused ion beam (FIB) of gallium ions in a FEI Helios NanoLab 600 DualBeam scanning electron microscope (SEM). The cantilevers ranged in size from about 0.5×1 to $3 \times 6\ \mu$m^2. Most of the cantilevers were aligned with their fixed end at the edge of the silicon and their free ends over the opening in the silicon support structure, as shown in Fig. 3. The first boundary condition in Fig. 2 was intended to model these cantilevers. Other cantilevers were formed by cutting past the edge of the silicon so that their fixed end was not at the edge of the silicon, but one or more micrometers back. The boundary condition for this second type of cantilever should be similar to the second or third case from Fig. 2, depending on how well adhered the MLG is to the silicon support structure. In both cases, this process results in cantilevers that can be freely deflected downward by AFM even to the large deflections needed for breaking (several hundred nanometers). However, the transfer process may not completely fix the end of the cantilever to the silicon because of the incomplete adhesion of the film to the silicon support. In order to increase the stiffness of the fixed end so that the cantilever deflects more like a fixed-free cantilever, some cantilevers had platinum bars deposited on the MLG where the cantilever meets the silicon. This was done using electron beam induced deposition of platinum in the dual beam SEM where the FIB cutting was performed. The width of each cantilever was measured by both AFM and SEM.

C. Thickness measurements

Min and MacDonald[18] and Zhu *et al.*[19] showed that the optical transmittance through multilayer graphene can be approximated with $T = (1 + f(\omega)\pi\alpha N/2)^{-2}$, where α is the fine-structure constant and $N = t/t_0$ is the number of graphene layers. Zhu *et al.* determined $f(\omega)$ to be 1.13 for 550 nm light and concluded that this was a good value for the visible range. With each graphene layer having a thickness of $t_0 = 0.335$ nm, this equation can be solved for thickness (in nanometers) as a function of transmittance,

$$t = \frac{2t_0}{f(\omega)\pi\alpha}\left(\frac{1}{\sqrt{T}} - 1\right) = 25.86\left(\frac{1}{\sqrt{T}} - 1\right). \quad (1)$$

An optical transmittance map of the film was measured as follows: three-channel color images were taken using an Olympus BX60F5 microscope with a tungsten halogen lamp and a Sony α7II 14-bit digital camera with a linear response (RAW format). The linearity of the camera sensor was confirmed with a series of neutral density filters and a constant intensity light source. The digital camera's settings were fixed to ensure no saturated pixels before taking an image without the MLG to record the intensity of the incident light. A second image was taken to record the intensity of the transmitted light through the suspended MLG film. The intensity of the halogen lamp was not changed between images. Care was taken to minimize extraneous light by turning off the room lights and illuminating the sample through an aperture. The green channel of the second image (MLG transmission intensity) was divided

by the green channel of the first image (incident intensity). The result was an image with pixel values representing transmittance according to $T = \Phi/\Phi_0$, where Φ is the intensity of the transmitted light and Φ_0 is the intensity of the incident light. The green channel was chosen because its peak sensitivity is closest to the 550 nm wavelength used by Zhu *et al.* A thickness map was created by applying Eq. (1) to each pixel in the transmittance image.

As an independent verification of film thickness, the film was also measured with a Bruker Dimension V atomic force microscope (AFM). With the MLG lying flat on the silicon substrate, an edge of the MLG film was found and the step height from the silicon to the film was measured in several places. This method can be used to estimate an average film thickness, but the measurement is always performed at the edge of the film, far away from the suspended area. Due to the non-uniformity of the films, the step height measurements alone are not sufficient for determining the thickness at the location of the cantilevers.

D. Mechanical testing

The force–deflection or beam bending method for determining the Young modulus of a material is performed by measuring and analyzing the deflection of a cantilever vs applied force. According to the Euler–Bernoulli beam theory, the stiffness k of a cantilever with one fixed end and one free end is related to its geometry and the Young modulus of the material,[21]

$$k = \frac{Ewt^3}{4L^3}, \tag{2}$$

where E is the Young modulus, w is the cantilever width, t is the cantilever thickness, and L is the distance from the fixed end of the cantilever to the applied force. The breaking strength is found by increasing the applied force until the cantilever breaks. The maximum stress at breaking σ_{max} is given by

$$\sigma_{max} = \frac{6FL}{wt^2}, \tag{3}$$

where F is the magnitude of the applied force.[21] Shear stress $\tau \approx 3F/2wt$ can be ignored when $\tau \ll \sigma_{max}$, which occurs when $L \gg t/4$. For our cantilevers with $t = 72$ nm, shear stress is ignored because the lengths are much greater than 18 nm. A disadvantage of the standard force–deflection method is that an independent measurement of L is needed. This measurement can be difficult because of the uncertainties in both the location of the fixed end and the location of the applied load. When using an AFM, the force is applied by the AFM cantilever tip, but there is no intrinsic measurement of where the tip contacts the sample relative to the fixed end of the cantilever. A modification to the standard force–deflection method involves deflecting the cantilever at multiple locations along its length and fitting both Young's modulus and an offset in the position of the applied force. As mentioned in the Introduction, we call this the multipoint force–deflection (MFD) method. This modification alleviates the requirement of an independent measurement of L. MFD does require, however, multiple force–deflection ramps with known spacing along the cantilever. Conveniently, automated force–volume mapping with an AFM results in a two-dimensional array of evenly spaced force–deflection ramps. Force–volume mapping was used to measure Young's modulus, while single force–deflection ramps were used for measuring strength.

1. force-volume measurement

On a Bruker Dimension V atomic force microscope, a force–volume (FV) measurement consists of capturing a square array of force–deflection ramps. After the region of interest is found using tapping mode imaging, the FV scan is set up with a specific trigger threshold for the force–deflection ramp. The ramp is engaged and, once that trigger value is reached, the ramp is reversed and the data for both the approach and retract ramps are saved. This is done for each point in the FV map. The stiffness of the AFM cantilever must be similar to that of the MLG cantilever. If it is too stiff, the AFM will not detect any displacement, and if it is too compliant, almost all of the displacement will be in the AFM cantilever and not the MLG cantilever. It is necessary to calibrate the force ramp against a much stiffer surface, such as the silicon support structure. This can be done by taking a single force ramp measurement on a stiff surface either before or after the FV measurement. It is also possible to use some of the FV data for the calibration, as long as part of the MLG in the scan is in direct contact with the silicon support structure. The average slope of the force ramps on the MLG over the silicon was used as the calibration factor for the data presented in this study. The calibration factor converts the recorded tip deflection from volts to nanometers and is often called the tapping mode deflection sensitivity. To convert this to a force, the AFM cantilever stiffness must be determined as described in Sec. II D 2. Most of the data in this work were captured in 64 × 64 pixel maps. With the fast scan setting enabled, each FV map took about 35 min to acquire. The FV data can be represented as a two-dimensional image by using the slope of a certain region of each of the force–deflection curves to represent the image intensity. Such an image would be called a stiffness map, and its inverse, a compliance map. Figure 4 shows a typical FV dataset represented as a compliance map, along with two force–deflection curves.

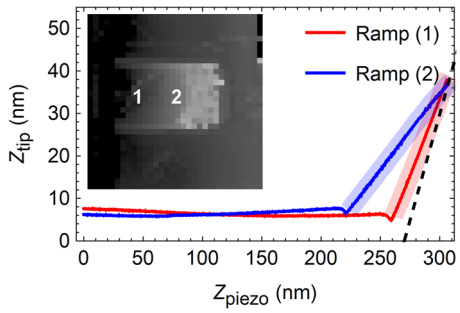

FIG. 4. Compliance map of an MLG cantilever and two different force–deflection ramps. The slope used in the analysis is taken from the light blue and pink highlighted linear regions of the force–deflection curve. The dashed black line has a slope of 1, representing a location with no compliance. (Inset) force–volume compliance map, where the intensity represents the local compliance of the film, which is inversely related to the slope of the force–deflection curve. Ramp (1) is closer to the fixed end than Ramp (2).

2. Analysis of force–volume data

The force–volume data consist of multiple force–deflection curves, from which several are selected, converted to compliance, and analyzed as a group to yield a Young's modulus. The force–deflection ramps along the centerline of the cantilever from the fixed end to the free end were selected for the analysis. The exact location of the fixed end is uncertain because of the poorly defined boundary between the cantilever and the silicon support; however, the MFD method does not require *a priori* knowledge of the fixed end location because an offset is fit. Each force–deflection ramp consists of three regions corresponding to pre-contact with the AFM cantilever, transition to contact, and contact. For an ideal force curve, the part corresponding to contact with the AFM cantilever will be linear, as shown in the highlighted regions in Fig. 4. The slope s of the linear portion can be related to the stiffness of the MLGC (many-layer graphene cantilever). This relationship is found by considering the interaction between the AFM cantilever and the MLGC as a system of two springs, as presented in Fig. 5. The total displacement $z_{piezo} = z_{tip} + z_G$ is the sum of the displacements of the AFM cantilever, z_{tip}, and the MLG cantilever, z_G. The force on the MLGC is equal to the force on the AFM cantilever, $F_G = k_G z_G = F_{tip} = k_{tip} z_{tip}$. Here, we work with compliance (the inverse of stiffness), in which case $k_G^{-1} = k_{tip}^{-1} z_G / z_{tip} = k_{tip}^{-1}(z_{piezo} - z_{tip})/z_{tip}$ or

$$\text{Compliance} = \frac{1}{k_G} = \frac{1}{k_{tip}}\left(\frac{1}{s} - 1\right), \tag{4}$$

where $s = z_{tip}/z_{piezo}$. Compliance is used to fit to the modified Euler–Bernoulli beam equation,

$$\frac{1}{k_G} = \frac{4(L-c)^3}{Ewt^3}, \tag{5}$$

where $1/k_G$ is the compliance of the MLG at the measured loading point, L is the position of the applied load relative to some initial visual estimate, c is an offset in the applied load position, E is the Young modulus, w is the MLGC width, and t is the MLGC thickness. The data were fit to Eq. (5) using a weighted nonlinear fitting function in Mathematica 12.2. The weight for each measurement point was calculated from the uncertainty in both k_G and L as $\delta = \sqrt{\delta k_G^{-2} + \delta L^{-2}}$. Equation (5) can also be fit with a linear regression by taking the cube root of both sides before fitting.

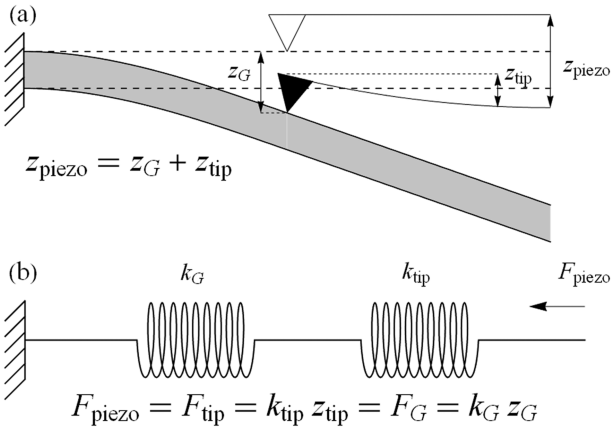

FIG. 5. Model of the interaction between the AFM cantilever and the MLG cantilever. (a) The deflection model shows that the deflection of the AFM piezo is the combined deflection of the AFM tip and the MLG cantilever. (b) The spring model allows for the transformation from the deflection model to the stiffness or compliance model.

The stiffness of the AFM cantilever, k_{tip}, can be estimated in multiple ways. One method is to use vibrometry to measure the resonance of the AFM cantilever, but the thickness must be known. The AFM cantilever thickness is variable, and measuring the thickness of each fragile tip requires handling that could damage the tip. A method was developed by Sader *et al.*[22] that simplifies estimating the stiffness of an AFM cantilever. Sader *et al.* classified the same type of tip that we used (NanoWorld NCHR); because of this, we can use their model if we know tip length, tip width, tip resonant frequency, quality factor, air density, and air shear viscosity. We used $\rho = 1.018$ kg/m^3 and $\mu = 1.813 \times 10^{-5}$ Pa · s for density and shear viscosity, respectively. The tip resonant frequency and quality factor were measured with the AFM before each force–volume measurement. The tip length and width were measured with an optical microscope for each AFM cantilever.

E. Raman spectroscopy of suspended MLG before and after FIB cutting

Raman spectroscopy was used to characterize the many-layer graphene films.[23,24] In the analysis of graphene by Raman spectroscopy, the three main peaks of interest are called D, G, and 2D and are located at Raman shifts of 1350, 1580, and 2700 cm^{-1}, respectively. The D peak indicates disorder in the graphene crystal. The lower the intensity of this peak, the higher the quality of graphene. The ratio of intensities of the G peak to the 2D peak gives an indication of the number of graphene layers in the film. For monolayer graphene, the G peak is smaller than the 2D peak. Conversely, for multilayer graphene and high quality graphite, the G peak is larger than the 2D peak. In this study, Raman spectroscopy was used to characterize the quality of the MLG films. Using a Renishaw inVia Raman spectroscopy microscope, the Raman spectra were measured for MLG both before and after cutting the cantilevers with the focused ion beam. A 532 nm laser (Renishaw RL532C50) and a 50× objective resulted in a laser spot size ~1 μm in diameter. A diffraction grating for visible light with 1800 lines per millimeter was used.

III. RESULTS

Finite element modeling of a cantilever with the three different boundary conditions described in Fig. 2 shows agreement between the first two boundary conditions and the analytical Euler–Bernoulli model. As expected, the third boundary condition does not match the analytical model. Two suspended MLG films were prepared with FIB cut cantilevers. The local thickness was measured near the cantilevers to be about 72 nm for one film and 160 nm for the other. The average Young's modulus was about 300 GPa, with a breaking strength of about 12 GPa. The focused ion beam used to create the cantilevers caused changes in the films, as evidenced by the formation of a strong D peak in the Raman spectra after ion-cutting.

A. Finite element modeling

The finite element modeling (FEM) results of cantilevers with the three different boundary conditions were compared, as described in the Methods (see Fig. 2). Deflection as a function of applied force is shown in Fig. 6 for the finite element solutions of all three models and the analytical (Euler–Bernoulli) solution. For the first two models, the calculated modulus was E_{FEM} = 1.01 TPa, which is within 1% of the value used for the FEM analysis. This 1% discrepancy may be the difference between the one-dimensional Euler–Bernoulli model and the three-dimensional FEM model. However, for the third boundary condition, the calculated modulus was E_{FEM} = 0.89 TPa. This method also returns an offset in the fixed end location. The offset for each boundary condition was −0.01, −0.02, and −0.2 μm, respectively, and relative to the start of L_0 in Fig. 2. The negative value indicates that the MFD method estimates the fixed end to be to the left of the given origin, using the orientation of the cantilever extending to the right. The offset for the third boundary condition was less than 10% of the total cantilever length. This source of error will be compared to other sources in the Discussion.

B. Suspended many-layer graphene film fabrication and preparation

Films were grown on two separate nickel foils that were then transferred onto silicon support structures, resulting in two samples: samples A and B. Platinum bars were deposited as stiffeners at the edge of the silicon on sample A. The platinum thickness was around 200 nm. Micrographs of the two films (after FIB cutting) are shown in Fig. 7. Sample A was placed on a silicon support structure with an open area of 120 × 620 μm^2, while the silicon support structure for sample B had a larger open area of 530 × 3020 μm^2.

A gallium ion beam was used to cut cantilevers in the MLG films, as shown in Fig. 7. A 1 × 1 μm^2 cantilever could be cut in about 5 s with an accelerating voltage of 30 kV and a beam current of 0.44 nA. In order to find the desired location for cutting the cantilevers, at least one rastered ion beam image was taken. The number of exposures and the exposure time were limited to minimize damage to the surrounding film. Exposing cantilevers to sufficient ion radiation would cause them to curl up. Cantilevers with significant curls were not included in the study. Several dozen cantilevers were cut into both samples; however, not all of the cantilevers were used in the study. Cantilevers that were not included did not cut cleanly or were not well aligned with the edge of the silicon.

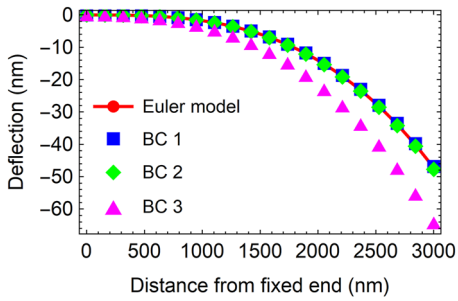

FIG. 6. Cantilever deflection results from finite element analysis. The three boundary conditions (BC 1–3) are introduced in Fig. 2. Both BC 1 and BC 2 match the analytical results of the Euler–Bernoulli beam model. BC 3 diverges significantly, as expected.

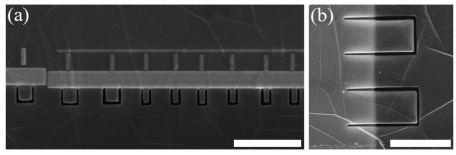

FIG. 7. Scanning electron micrographs of MLG with cantilevers. (a) Cantilevers from sample A with a platinum bar stiffener, going from 1 × 1 μm^2 on the left to 0.5 × 1 μm^2 on the right. The thicker horizontal bar above the cantilevers is the platinum stiffener. The thinner vertical and horizontal bars are navigation markers for AFM. (b) The two cantilevers from sample B, which lack a platinum stiffener. The lighter tone in the left half of the image is from the silicon underneath the MLG. The cut forming the cantilever extends back onto the silicon, resulting in a cantilever that is significantly shorter than the total cut length, if the cantilever hits the silicon edge while deflecting downward. The cuts form a cantilever that is 3 × 6 μm^2, with the part extending past the silicon being about 3 × 3.5 μm^2. The scale bars are 5 μm long.

C. Thickness

The MLG film thickness was measured both with an optical transmittance technique and by AFM step height. Figure 8 shows the thickness results for the two samples in the study. Figures 8(a)–8(c) show the thickness maps for sample A (a) and sample B (b) and (c). Figure 8(d) shows the thickness distributions for all of (a) in red, all of (b) in blue, and the highlighted part of (c) in green. Gaussian functions were fit to the distributions in Fig. 8(d). The location of the peak of the Gaussian and its standard deviation were taken to be the thickness and uncertainty, respectively. For sample A [the red curve in Fig. 8(d)], which was relatively uniform in thickness, the result of the optical transmittance measurement was (72 ± 7) nm. Additionally, step height measurements with the AFM ranged from 68 to 73 nm. One such a step height scan is shown in Figs. 8(e) and 8(f). Sample B has two distinct thickness regions, as shown in the left and right halves of Fig. 8(b). The blue curve in Fig. 8(d) is the thickness distribution for both regions, and the green curve is the distribution of just the region near the cantilevers [as highlighted in Fig. 8(c)]. The thickness distribution of all of sample B [Fig. 8(b)] peaked at 55 nm. Two Gaussians were fitted to the distribution from Fig. 8(c), resulting in thicknesses of (120 ± 10) and (160 ± 20) nm. The 160 nm peak was chosen for the analysis because it was more prominent. The AFM step height measurements for sample B ranged from 80 to 105 nm. These step heights were taken at the edge of the film, far from the cantilevers.

D. Young's modulus

Young's modulus was determined using 30 force–volume scans of 20 unique cantilevers from sample A. The average Young's modulus was (300 ± 20) GPa, where the uncertainty is the standard error (standard deviation divided by the square root of the number of samples). See the supplementary material of this paper for details on repeated measurements. Representative force–volume compliance maps from samples A and B are shown in the insets of Figs. 9(a) and 9(b), respectively. Also shown are graphs of the compliance as a function of position along the cantilever, as well as the fitted line

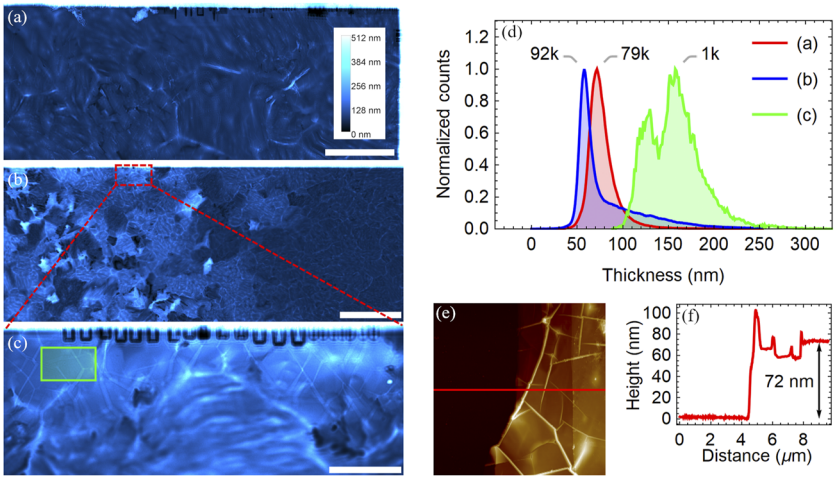

FIG. 8. Thickness results for samples A and B. (a) Thickness map of sample A at 50×, with cantilevers visible near the top of the image. The scale bar is 25 μm. (b) Thickness map of sample B at 5×. The scale bar is 200 μm. (c) Thickness map of sample B at 50× with cantilevers visible near the top of the image. The scale bar is 25 μm. (d) Thickness distribution of (a) and (b) and of the region highlighted in green of (c). The peaks are marked with their original count values, which were used for normalization. (e) AFM step height scan of sample A. The scan is 10 μm square. (f) Height profile from scan in (e) showing 72 nm thickness.

(blue) from which Young's modulus was extracted. The compliance map in Fig. 9(b) shows a jump in compliance near the middle of the cantilever. This is one of several non-ideal features in the cantilevers of sample B that are important to understand and will be addressed in the Discussion.

The offset in the fixed end position was significantly different between samples A and B, as shown in Fig. 9(c). A fixed end offset closer to zero means that the visual estimate for the location of the fixed end more closely matched the value from fitting. A negative offset means that the fit value was estimated to be to the left of the

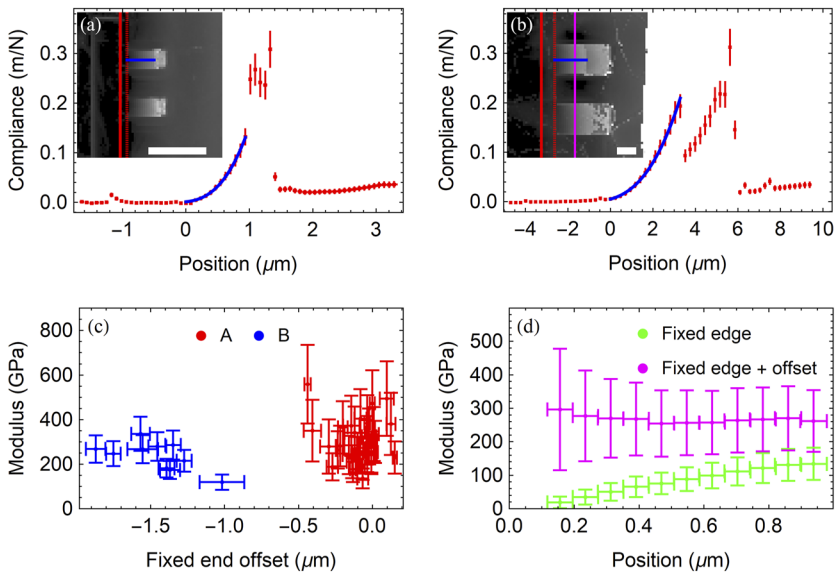

FIG. 9. Results of Young's modulus measurements and calculations. (a) The inset shows a compliance map with two cantilevers from sample A. Lighter areas are more compliant. The horizontal blue line across the center of the top cantilever marks the location used for the MFD analysis and covers the same region as the blue line in the compliance plot. The solid vertical red line shows the position of the cantilever fixed end estimated by fitting, while the dashed red line shows the visual estimate of the cantilever fixed end. (b) Compliance map and plot from sample B [see (a) for the description of each]. The solid magenta line marks the silicon edge, as determined by SEM [see Fig. 7(b)]. A jump in compliance immediately to the right of the blue line can be seen in both the map and the plot. The force–deflection curves (from which compliance is extracted) near the free end of the cantilevers and near the right edge of the map were often too noisy to extract meaningful data and hence the white pixels. (c) Each crosshair is the fitted Young's modulus plotted against the fitted fixed end offset of a single cantilever. The offset is the distance from the visual fixed end of the cantilever to the fixed end determined by fitting. (d) The single-point force–deflection method at each point along the cantilever from (a) using the visual estimate of the fixed edge (green) and the fixed edge with the offset (magenta) found in (c). Without the offset, the value of the calculated modulus changes as a function of position along the cantilever. With the offset, the value of the modulus is independent of the position along the cantilever, highlighting one of the benefits of the multipoint force–deflection method. The scale bars for the compliance maps in the insets of (a) and (b) are 2 μm long.

cantilever's fixed end, according to the orientation in the compliance maps of Figs. 9(a) and 9(b).

Figure 9(d) shows the results of using the single-point force–deflection method independently at each loading position. This method uses only a single loading to estimate Young's modulus and so has no way to estimate the offset in the cantilever's fixed end position. Two different cases are shown. In the first case (green), Young's modulus is underestimated because our visual estimate for the fixed end location is not correct and an offset is not used. This also leads to the determined Young's modulus changing at different positions along the cantilever. In the second case (magenta), the offset estimated from the MFD method is used, resulting in a position independent estimate of Young's modulus. The range in moduli for the first case is 100 GPa, while it is only 10 GPa for the second case. The largest relative error in modulus for any of the points in Fig. 9(d) by the single-point method is 60%. The same sample analyzed with the MFD method returned a relative error of 20%.

E. Strength

To measure the strength of the films, five cantilevers from sample A were deflected until fracture. The forces required to break the cantilevers ranged from 11 to 25 μN. According to Eq. (3), the resulting strength is (12 ± 2) GPa, with the uncertainty being the standard error. Figure 10(a) shows the force–deflection ramp of a cantilever that broke at about 13 μN, with the broken cantilever pictured in Fig. 10(b). A fracture is visible at the fixed edge of the cantilever along the platinum bar. The force required to break the cantilever is far beyond its region of linear response, as seen from the changing slope in the force–deflection ramp. Each cantilever deflected several hundred nanometers before fracturing. With such a high deflection, the angle between the cantilever and the AFM tip was large, facilitating tip slippage. We did not include nonlinear effects or tip slippage in our analysis because we did not have a method to quantify the position of the AFM tip after slipping.

F. Focused ion beam induced changes in film

Raman spectroscopy was used to characterize the quality of the CVD films, as shown in Fig. 11(a). There is little evidence for the D peak (1350 cm^{-1}) in films before FIB cutting or in areas of the film far from the FIB cutting. However, a strong D peak does form in areas near the MLG cut by the FIB. Figure 11(b) shows a scanning transmission electron microscope (STEM) annular ring dark-field image captured with a FEI Verios G4 SEM. The contrast of the image is representative of the angle at which electrons scattered through the film. Near the cantilevers (top and right), the contrast is more uniform. It is clear that the topology of the film is different in these regions than in the rest of the film. These areas were exposed to ion beam imaging during FIB cutting.

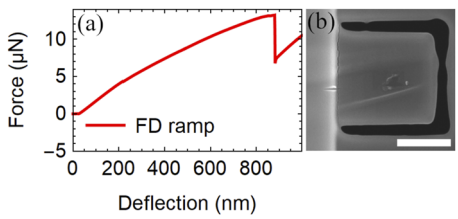

FIG. 10. Representative force–deflection ramp until failure and the fractured cantilever. (a) force–deflection ramp of a cantilever that was loaded until fracture. (b) SEM image of a cantilever with a small crack that formed at the fixed end. Markings from the AFM tip are visible near the center of the cantilever and at the fixed end. The scale bar is 0.5 μm long.

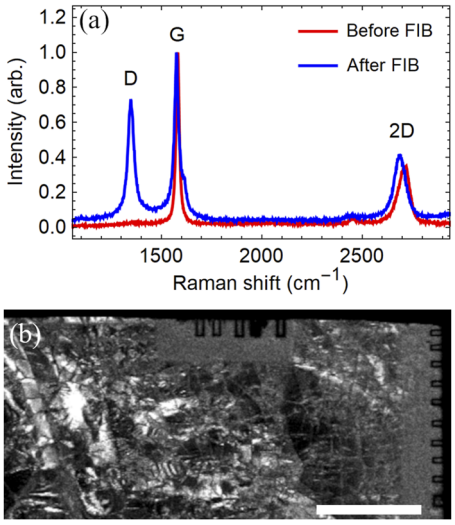

FIG. 11. Ion beam induced changes to MLG film. (a) Raman spectra before (red) and after (blue) processing with the focused ion beam. The spectra were normalized to their respective G peaks. Before ion beam processing, there is little to no observable D peak. A large D peak is present after processing. The D peak is indicative of the graphitic disorder. (b) Scanning transmission electron microscopy dark-field image with a 10 μm scale bar. The film near the cantilevers exhibits a greater uniformity than the film farther away, indicating that the ion beam had a transformative effect on the MLG near the cantilevers.

IV. DISCUSSION

The finite element modeling results highlight the importance of understanding the cantilever boundary conditions and justify the use of a simple Euler–Bernoulli cantilever beam model for samples with a well-defined fixed end. The modeling results show only a small difference in deflection between the Euler–Bernoulli analytical model and the first two boundary conditions of the FEM (see Fig. 6), leading us to conclude that the MFD can be used to extract Young's modulus for a cantilever with a well-defined fixed end. When the fixed-free cantilever analysis associated with BC 1 is applied to BC 3, the fit offset that results is less than 10% of the cantilever length. Consequently, we do not believe that a fit offset significantly larger than 10% can be explained solely by a difference in the local clamping geometry. Using knowledge from microscopy (AFM or SEM) of the fixed end location, we excluded from further analysis cantilevers whose fit offset was significantly larger than 10% of the cantilever length, as explained in the following paragraphs.

A significant benefit of the multipoint force–deflection method is that it allows for an independent determination of the location of the cantilever's fixed end. Not only do the compliance maps provide a visual estimate of the fixed end location, but the MFD analysis itself

also returns a fixed end offset along with the estimate of Young's modulus (see the insets of Figs. 4 and 9). If the location of the fixed end is known with some confidence, then MFD's fixed end offset can be used to justify or reject the chosen model, as described in the following two paragraphs.

The cantilevers in sample A had a platinum bar stiffener deposited at their fixed end. The stiffeners were an attempt to create a more ideal fixed end to enable the MFD analysis using a simple fixed-free Euler–Bernoulli beam model. The results show that cantilevers with a stiffener had a smaller fixed end offset than cantilevers without a stiffener [see Fig. 9(c)]. The fixed end offset and the visual estimate of the cantilever fixed end location were similar, indicating that the base of the cantilever acted like a fixed end, justifying, in practice, the use of the simple Euler–Bernoulli beam model that enables the MFD analysis.

The analysis by MFD of the cantilevers in sample B is complicated by their geometry and their lack of stiffeners. Figure 7(b) shows that about half of the cut length is past the edge of the silicon. We expected the cut part of the MLG film over the silicon to have little compliance based on the assumption that the film and silicon would be in contact. However, it was clear from the force–volume map that the entire cut portion of the cantilever was compliant and was not in direct contact with the silicon [see Fig. 9(b)]. This indicates that the cantilever was curled upward or otherwise not in contact with the silicon, a condition not accounted for in the analytical model or in the finite element model. We believe that the jump in compliance observed in Fig. 9(b) was caused by the cantilever deflecting enough to contact the silicon in another location, possibly at the silicon edge. See the supplementary material for a further discussion of this jump in compliance. In addition, the cantilevers in sample B had a fairly large discrepancy between our best visual guess at the location of their fixed end and the fixed end predicted by the MFD analysis. Despite a good fit to Eq. (5), the estimated location of the fixed end would indicate a cantilever much longer than the cut cantilever [see Fig. 7(b)], leading us to conclude that the actual boundary condition is more complicated than any of our models. The lack of a good model for the cantilevers in sample B precludes the MFD analysis for the determination of Young's modulus.

When MFD data can be fitted using the Euler–Bernoulli model, it can further reduce experimental uncertainties. With single-point force–deflection, any error in the location of the applied load is propagated to Young's modulus [see Eq. (2)]. However, with MFD analysis, an error in location (i.e., an offset) affecting all loading points equally is removed by the fixed end offset [see Eq. (5)]. An error affecting loading points differently, such as an error in the force–volume step size ΔL [see Fig. 1(b)], will still affect the modulus.

The fixed-free cantilever beam is not the only geometry where MFD is possible. Other authors have previously reported a similar technique that uses a doubly clamped beam model.[9,10,25] Fixed-free cantilever beams were easier to fabricate than doubly clamped beams in our samples because they only require one fixed edge and our silicon support structures had very large openings. The fixed-free beam model also has an advantage over a doubly clamped beam because it depends solely on bending rather than on bending and tension.

MFD is a technique for local measurements of Young's modulus that requires a complementary technique for locally measuring thickness. To take advantage of the local nature of the MFD method, it is necessary to know the thickness at the site of the cantilever. For example, the average thickness of sample B was about 55 nm. However, the cantilevers we tested were in a much thicker region of the film, which we were able to measure with an optical transmittance technique to be about 160 nm (see Fig. 8). Uncertainty in thickness is the largest source of error in these measurements. With Young's modulus $E \propto t^{-3}$, the uncertainty from thickness is $\delta E = 3|E|\delta t/|t|$. Using relevant magnitudes and errors as an example, if $E = 500$ GPa, $t = 70$ nm, and $\delta t = 5$ nm, then the uncertainty is $\delta E = 100$ GPa, giving a relative uncertainty of 20%. Other sources of uncertainty (and their relative errors) include cantilever width (1%), AFM tip stiffness (5%), AFM tapping mode deflection sensitivity (5%), and AFM lateral resolution (<1%). The finite element modeling showed that choosing a model with the wrong boundary condition (e.g., assuming BC 1 when BC 3 was more appropriate) would lead to an error of 10% for cantilevers with our geometry.

The optical transmittance technique for estimating the thickness of a MLG film is useful up to the resolution limit of the optical imaging system. With small cantilevers and sharp lines from wrinkles, diffraction plays a role and makes measuring the transmittance near the cantilevers or wrinkles difficult. Figure 8(c) suffers slightly from these effects. For thicker films, the transmittance is very low and can be buried in the background noise (i.e., from extraneous light). It is important to maximize the light transmitted through the film by ensuring that the intensity of the incident light is near the saturation limit of the detector. With a 14-bit sensor, the maximum measurable film thickness is $t = 25.856(1/\sqrt{1/2^{14}} - 1) = 3300$ nm. The background noise effectively decreases the bit depth of the sensor. The average background noise for our images (~380 ADC counts) decreased the maximum measurable thickness by just over 1%. This decrease is negligible because the measured thickness of our films was less than 200 nm. Other measurement techniques, such as spectroscopic ellipsometry and AFM step height measurements, are not feasible for measuring film thickness near the cantilevers.

The ion beam used to cut the cantilevers also caused changes to the surrounding film, which is a limitation of this work that can be addressed with other fabrication techniques as described below. These changes are evidenced by the large Raman D peak in the post-cut sample and by the lower contrast of the MLG near the cantilevers in the dark-field transmission images, both shown in Fig. 11. Another challenge with FIB cutting is the requirement of a careful alignment between the sample, the ion beam, and the electron beam. It is not possible to see through the MLG film with ion beam imaging in order to align the fixed edge of the cantilever to the silicon support edge, which is why alignment with the electron beam is necessary. Several samples had cantilevers that were too poorly aligned to be tested. It may be possible to protect the MLG film during FIB cutting by postponing the PMMA removal step until after the FIB process. PMMA is not electrically conductive, so a thin conductive layer, such as thermally evaporated carbon, could be deposited before processing in the electron microscope. Other methods for creating cantilevers in suspended thin films (or before the films are released) may reduce or eliminate both the challenges of alignment and of undesirable film modification. Optical and electron-beam lithography are two such methods. Lithographically patterned films can be etched with wet or dry processes. Other studies have shown that wet[26] and dry[4] etching methods can negatively impact graphene films but not to the extent that we have seen with ion bombardment.

The multipoint force–deflection method for determining Young's modulus has several advantages over other techniques, such as the single-point force–deflection method and bulge testing. First, by using multiple data points and fitting them to a model,[26,20] an independent measurement of the distance from the fixed end of the cantilever to the applied force is not necessary. This can simplify the measurement and remove one source of error. Second, MFD results give information about the boundary condition that can be used to justify or reject the model. MFD allowed us to differentiate between cantilevers with a well-defined fixed end and those without. Third, using MFD with microcantilevers allows for the measurement of local film properties in heterogeneous films, something that is not possible with bulge testing. We used the MFD method to determine the Young modulus of many-layer graphene films with a large thickness non-uniformity to be (300 ± 20) GPa. The strength was also estimated to be (12 ± 2) GPa. The measured Young's modulus is ~30% of that reported for pristine graphene and pyrolytic graphite,[11] which may be explained by an ion-induced modification to the film during cantilever fabrication. This limitation could potentially be overcome with other microcantilever fabrication methods, such as electron-beam lithography and wet or dry etching. The multipoint force–deflection method was shown to be well suited for measuring these non-uniform many-layer graphene films.

SUPPLEMENTAL MATERIAL

See the supplementary material for a description of the many-layer graphene fabrication process, brief discussions on the repeatability of MFD measurements and the jump in compliance from Fig. 9(b), and information on exporting force–volume data from the NanoScope Analysis software.

ACKNOWLEDGMENTS

We thank Paul Minson and Michael Standing of the BYU Microscopy Facility for their technical help with electron microscopy imaging and FIB cutting. We thank Brian Jensen for the discussion about beam equations and nonlinearity. We also thank Moxtek for providing initial project funding and for allowing us to use their facilities for the fabrication of the many-layer graphene samples.

AUTHOR DECLARATIONS

Conflict of Interest

The authors have no conflicts to disclose.

Author Contributions

Kyle Larsen: Conceptualization (equal); Formal analysis (lead); Investigation (lead); Methodology (equal); Visualization (lead); Writing – original draft (lead); Writing – review & editing (lead). **Stefan Lehnardt**: Investigation (supporting). **Bryce Anderson**: Investigation (supporting). **Joseph Rowley**: Conceptualization (supporting); Investigation (supporting). **Richard Vanfleet**: Conceptualization (supporting); Funding acquisition (equal); Supervision (equal); Writing – review & editing (supporting). **Robert Davis**: Conceptualization (lead); Funding acquisition (equal); Methodology (equal); Project administration (equal); Writing – review & editing (equal).

DATA AVAILABILITY

The data that support the findings of this study are available from the corresponding author upon reasonable request.

REFERENCES

[1] J. J. Vlassak and W. D. Nix, J. Mater. Res. **7**, 3242 (1992).
[2] T. P. Weihs, S. Hong, J. C. Bravman, and W. D. Nix, J. Mater. Res. **3**, 931 (1988).
[3] R. Rasuli, A. Iraji zad, and M. M. Ahadian, Nanotechnology **21**, 185503 (2010).
[4] P. Li, Z. You, and T. Cui, Appl. Phys. Lett. **101**, 093111 (2012).
[5] M. Poot and H. S. J. van der Zant, Appl. Phys. Lett. **92**, 063111 (2008).
[6] C. Lee, X. Wei, J. W. Kysar, and J. Hone, Science **321**, 385 (2008).
[7] G.-H. Lee, R. C. Cooper, S. J. An, S. Lee, A. van der Zande, N. Petrone, A. G. Hammerberg, C. Lee, B. Crawford, W. Oliver, J. W. Kysar, and J. Hone, Science **340**, 1073 (2013).
[8] K. K. Al-Quraishi, Q. He, W. Kauppila, M. Wang, and Y. Yang, Int. J. Smart Nano Mater. **11**, 207 (2020).
[9] G. Guhados, W. Wan, and J. L. Hutter, Langmuir **21**, 6642 (2005).
[10] G. Guhados, W. Wan, X. Sun, and J. L. Hutter, J. Appl. Phys. **101**, 033514 (2007).
[11] O. L. Blakslee, D. G. Proctor, E. J. Seldin, G. B. Spence, and T. Weng, J. Appl. Phys. **41**, 3373 (1970).
[12] H. I. Rasool, C. Ophus, W. S. Klug, A. Zettl, and J. K. Gimzewski, Nat. Commun. **4**, 2811 (2013).
[13] Q. Zhou and A. Zettl, Appl. Phys. Lett. **102**, 223109 (2013).
[14] S. Huebner, N. Miyakawa, S. Kapser, A. Pahlke, and F. Kreupl, IEEE Trans. Nucl. Sci. **62**, 588 (2015).
[15] S. Huebner, N. Miyakawa, A. Pahlke, and F. Kreupl, Phys. Status Solidi B **252**, 2564 (2015).
[16] S. Huebner, N. Miyakawa, A. Pahlke, and F. Kreupl, MRS Adv. **1**, 1441 (2016).
[17] J. Rowley, "Sp^2 bonded carbon for soft x-ray detector windows," Ph.D. dissertation (Brigham Young University, 2021).
[18] H. Min and A. H. MacDonald, Phys. Rev. Lett. **103**, 067402 (2009).
[19] S.-E. Zhu, S. Yuan, and G. C. A. M. Janssen, Europhys. Lett. **108**, 17007 (2014).
[20] J. W. Suk, A. Kitt, C. W. Magnuson, Y. Hao, S. Ahmed, J. An, A. K. Swan, B. B. Goldberg, and R. S. Ruoff, ACS Nano **5**, 6916 (2011).
[21] L. L. Howell, *Compliant Mechanisms* (John Wiley and Sons, 2001).
[22] J. E. Sader, J. A. Sanelli, B. D. Adamson, J. P. Monty, X. Wei, S. A. Crawford, J. R. Friend, I. Marusic, P. Mulvaney, and E. J. Bieske, Rev. Sci. Instrum. **83**, 103705 (2012).
[23] A. C. Ferrari and D. M. Basko, Nat. Nanotechnol. **8**, 235 (2013).
[24] D. G. Papageorgiou, I. A. Kinloch, and R. J. Young, Prog. Mater. Sci. **90**, 75 (2017).
[25] F. Traversi, F. Javier Gúzman-Vázquez, L. Giorgia Rizzi, V. Russo, C. Spartaco Casari, C. Gómez-Navarro, and R. Sordan, New J. Phys. **12**, 023034 (2010).
[26] E. Sandoz-Rosado, E. D. Wetzel, J. T. Smith, S. Oida, and J. Bai, in *2015 IEEE 15th International Conference on Nanotechnology (IEEE-NANO)* (IEEE, 2015), pp. 37–40.